International Journal of
Molecular Sciences

MDPI

Article

Proline Oxidation Supports Mitochondrial ATP Production When Complex I Is Inhibited

Gergely Pallag [1], Sara Nazarian [1], Dora Ravasz [1], David Bui [1], Timea Komlódi [2], Carolina Doerrier [2], Erich Gnaiger [2], Thomas N. Seyfried [3] and Christos Chinopoulos [1,*]

[1] Department of Biochemistry and Molecular Biology, Semmelweis University, 1094 Budapest, Hungary; pallag.gergely@semmelweis-univ.hu (G.P.); nazarian.sara@med.semmelweis-univ.hu (S.N.); ravasz.dora@med.semmelweis-univ.hu (D.R.); b.d4vid@gmail.com (D.B.)
[2] Oroboros Instruments, 6020 Innsbruck, Austria; timea.komlodi@oroboros.at (T.K.); carolina.doerrier@oroboros.at (C.D.); erich.gnaiger@oroboros.at (E.G.)
[3] Biology Department, Boston College, Chestnut Hill, MA 02467, USA; seyfridt@bc.edu
* Correspondence: chinopoulos.christos@med.semmelweis-univ.hu

Abstract: The oxidation of proline to pyrroline-5-carboxylate (P5C) leads to the transfer of electrons to ubiquinone in mitochondria that express proline dehydrogenase (ProDH). This electron transfer supports Complexes CIII and CIV, thus generating the protonmotive force. Further catabolism of P5C forms glutamate, which fuels the citric acid cycle that yields the reducing equivalents that sustain oxidative phosphorylation. However, P5C and glutamate catabolism depend on CI activity due to NAD^+ requirements. NextGen-O2k (Oroboros Instruments) was used to measure proline oxidation in isolated mitochondria of various mouse tissues. Simultaneous measurements of oxygen consumption, membrane potential, NADH, and the ubiquinone redox state were correlated to ProDH activity and F_1F_O-ATPase directionality. Proline catabolism generated a sufficiently high membrane potential that was able to maintain the F_1F_O-ATPase operation in the forward mode. This was observed in CI-inhibited mouse liver and kidney mitochondria that exhibited high levels of proline oxidation and ProDH activity. This action was not observed under anoxia or when either CIII or CIV were inhibited. The duroquinone fueling of CIII and CIV partially reproduced the effects of proline. Excess glutamate, however, could not reproduce the proline effect, suggesting that processes upstream of the glutamate conversion from proline were involved. The ProDH inhibitors tetrahydro-2-furoic acid and, to a lesser extent, S-5-oxo-2-tetrahydrofurancarboxylic acid abolished all proline effects. The data show that ProDH-directed proline catabolism could generate sufficient CIII and CIV proton pumping, thus supporting ATP production by the F_1F_O-ATPase even under CI inhibition.

Keywords: proline dehydrogenase; substrate-level phosphorylation; coenzyme Q; reducing equivalent

Citation: Pallag, G.; Nazarian, S.; Ravasz, D.; Bui, D.; Komlódi, T.; Doerrier, C.; Gnaiger, E.; Seyfried, T.N.; Chinopoulos, C. Proline Oxidation Supports Mitochondrial ATP Production When Complex I Is Inhibited. *Int. J. Mol. Sci.* **2022**, *23*, 5111. https://doi.org/10.3390/ijms23095111

Academic Editors: Anna Atlante and Daniela Valenti

Received: 29 March 2022
Accepted: 2 May 2022
Published: 4 May 2022

1. Introduction

Taggart and Krakaur discovered proline oxidation in mitochondria isolated from rabbit kidneys in 1949 [1]. In 1962, Johnson and Strecker reproduced this finding in rat liver mitochondria [2], and in 1986, McKnight and Hird demonstrated proline oxidation in mitochondria from other rat tissues [3]. Although proline oxidation has received the most attention in insect flight muscles [4–6], and pioneering studies by Phang and co-workers have established a specialized role for this amino acid in cancer metabolism [7,8].

Hereby, we investigated the effect of proline oxidation in providing sufficient bioenergetic drive for supporting mitochondrial ATP production when respiratory Complex CI, which was inhibited using rotenone. Being mindful that proline catabolism exhibits strong tissue-dependence, we measured the extent of proline oxidation in isolated mitochondria that was obtained from mouse liver, kidney, heart, and brain. Proline catabolism (and in particular ProDH activity) has only been investigated in mouse liver mitochondria to the best of our knowledge [9].

The metabolism of proline in mitochondria is outlined in Scheme 1 shown below. For a more detailed review see [10,11]. As shown in the scheme, proline enters mitochondria through a bi-directional transporter. Unlike the plasma membrane, in which twelve transporters have been identified and characterized [12], the transport of proline across the mitochondrial inner membrane has been regarded only as "energy-dependent" [13] and is mediated by two entities: a proline uniporter and a proline/glutamate antiporter [14]. The genetic identities of these transporters remain unknown. The rate of proline transport by these two mitochondrial transporters is similar to the first two steps of proline oxidation, indicating that transport is not a limiting factor for proline metabolism [13]. Once inside the matrix, the proline dehydrogenase/proline oxidase (ProDH) reversibly converts proline to pyrroline-5-carboxylate (P5C). There are two ProDH enzymes: ProDH1, which converts L-proline to P5C, and ProDH2, which catalyzes the conversion of hydroxyproline to pyrroline-3-hydroxy-5-carboxylate [15]. ProDH2 can also use proline as a substrate, but with much lower efficiency [15]. ProDH enzymes are FAD-bound, thereby reducing UQ [9,16]. In 1965, Erecińska identified the requirement of ubiquinone in proline oxidation [17]. Reduced Q (ubiquinol, UQH_2) fuels CIII, subsequently transferring electrons to CIV—provided that a suitable final electron acceptor is available [9]. P5C non-enzymatically tautomerizes to glutamate semi-aldehyde (GSA). GSA may have two fates: (i) transamination with glutamate to ornithine and oxoglutarate (Og; α-ketoglutarate) by ornithine aminotransferase (OAT), and/or (ii) oxidation to glutamate by delta-1-pyrroline-5-carboxylate dehydrogenase (ALDH4A1) concomitantly reducing $NAD(P)^+$ to NAD(P)H. Glutamate may then enter the citric acid cycle either through glutamate dehydrogenase yielding oxoglutarate, or through transamination with oxaloacetate to oxoglutarate and aspartate by aspartate aminotransferase (ASAT).

Being mindful of the above metabolic considerations, we investigated the effects of adding proline to mitochondria by measuring: (i) oxygen consumption (final electron acceptor of CIV that receives electrons from CIII fueled by UQH_2 generated by ProDH), (ii) NAD^+ reduction reflecting ALDH4A1, GDH, and citric acid cycle dehydrogenases activities, (iii) ubiquinone reduction by ProDH while converting proline to P5C, (iv) generation of a mitochondrial membrane potential ($\Delta\Psi_{mt}$) by CIII and CIV proton pump activity, and the subsequent use of these protons by F_1F_O-ATPase and downstream events that alter matrix ATP/ADP (in the presence of CI inhibition), and (v) the directionalities of F_1F_O-ATPase and the adenine nucleotide translocase (ANT), which are profoundly influenced by the ATP/ADP ratio, [18]—also in the presence of CI inhibition. Data obtained from these experiments were correlated with ProDH activity values that were estimated from the same tissues.

We report that proline could maintain ATP formation by the mitochondrial F_1F_O-ATPase under CI inhibition only in tissues with high ProDH activity. This effect was mediated by the reduction of ubiquinone (UQ) fueling Complexes CIII and CIV, which in turn generates a membrane potential that is not due to the oxidation of glutamate and is formed by the catabolism of proline. Our results suggest that proline catabolism can bypass a CI blockade, thus preventing bioenergetic collapse.

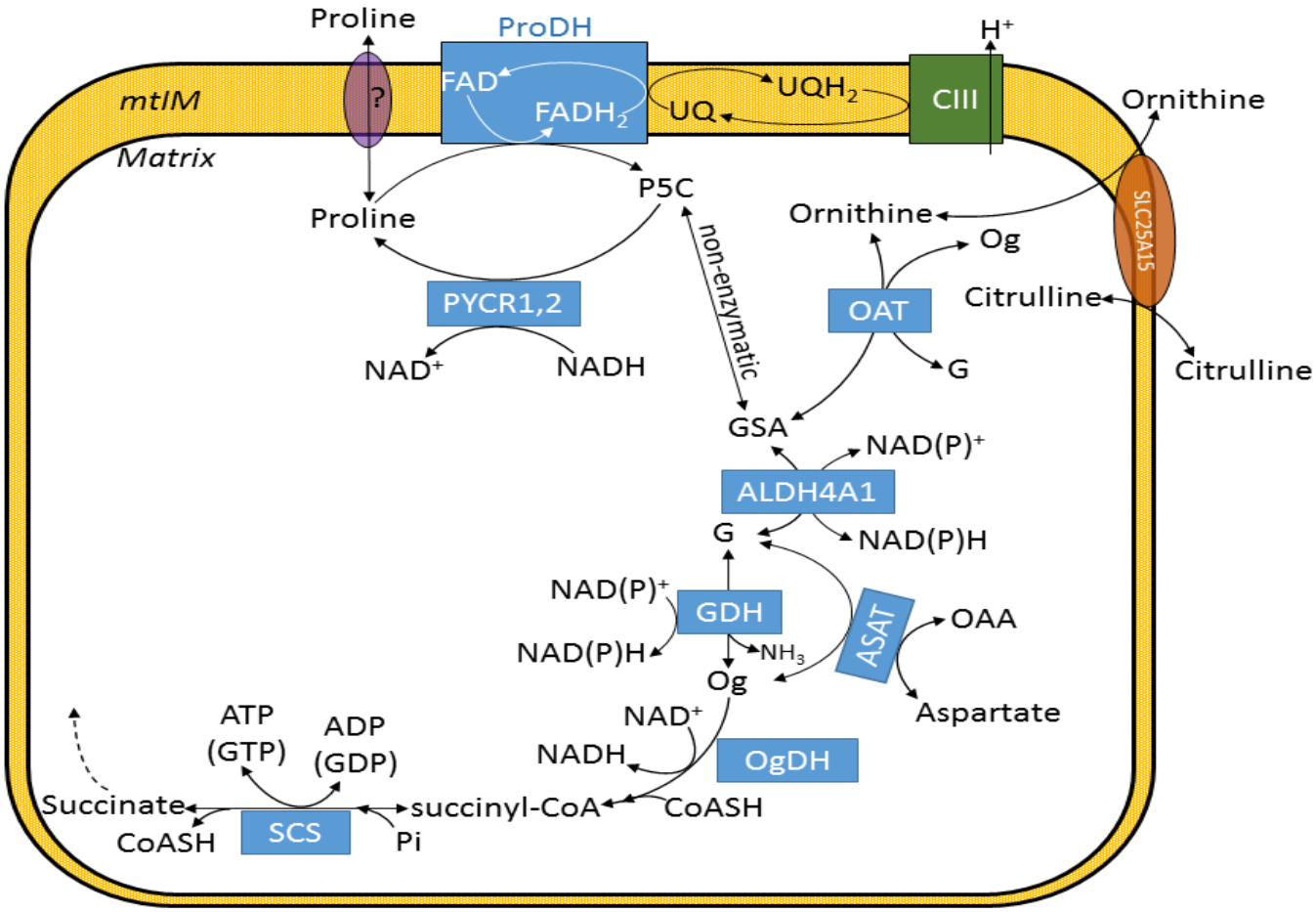

Scheme 1. The pathway of proline metabolism. Og: oxoglutarate; ALDH4A1: Aldehyde Dehydrogenase 4 Family Member A1 (L-Glutamate Gamma-Semialdehyde Dehydrogenase); ASAT: aspartate aminotransferase; CIII: Complex III; G: glutamate; GDH: glutamate dehydrogenase; GSA: glutamate semi-aldehyde; mtIM: mitochondrial inner membrane; OAA: oxaloacetate; OAT: ornithine aminotransferase; OgDH: oxoglutarate dehydrogenase; P5C: pyrroline-5-carboxylate; ProDH: proline dehydrogenase; PYCR1,2: pyrroline-5-carboxylate reductase isoforms 1 or 2; SLC25A15: solute carrier family 25 member 15; SCS: succinate-CoA ligase (succinyl-CoA synthetase).

2. Results

2.1. Kinetic Characterization of Proline Dehydrogenase in Mitochondria Isolated from Various Mouse Tissues

To the best of our knowledge, ProDH activity in murine tissues has onlybeen reported from a mouse liver model [9] and various organs of rats [3]. Thus, we first measured ProDH catalytic activity content in isolated mitochondria from mouse liver, kidney, brain, and heart, and also determined the apparent K_m of mouse liver ProDH for proline. As shown in Figure 1A, liver and kidney mitochondria exhibited much higher ProDH activity than brain and heart mitochondria, as similarly reported for rat tissues in [3]. We further determined the apparent K_m of ProDH for proline in mouse liver mitochondria and report it to be 3.08 ± 0.48 mM (Figure 1B), which was estimated by non-linear fitting. Values of 2.4 mM for fetal and adult rat liver mitochondria [19] and 0.42–1.2 mM in DLD-POX cells [9] have been previously reported.

2.2. Liver and Kidney Mitochondria Respire on Proline

Having measured the tissue-dependent ProDH activity in isolated mitochondria from mouse tissues, we sought to establish the extent of proline catabolism as a respiratory substrate. The effect of proline on oxygen consumption rates (and all subsequent experiments)

was tested in the 0.25–10 mM concentration range. This is because the normal human plasma concentration of this amino acid is in the range of 100–250 µM [13,20–23]. However, in patients suffering from type 2 diabetes, obesity, insulin resistance [24], or cancer-associated cachexia [25], an almost two-fold increase has been reported. Similar to humans, plasma proline concentration in the range of 0.25–0.3 mM has been observed in rats [26].

As shown in Figure 1C for liver and 1H for kidney, proline led to a dose-dependent (0.25–10 mM) increase in LEAK and OXPHOS respiration (kinetically saturating ADP [27]) of isolated mitochondria. The proline-induced increases in LEAK and OXPHOS respiration were, however, masked if glutamate and malate (Figure 1D for liver and 1I in kidney); glutamate, malate, and β-hydroxybutyrate (βOH, Figure 1E in liver); or glutamate, malate, and itaconate (Figure 1J in kidney) were present. βOH increases the NADH/NAD^+ ratio due to the high activity of β-hydroxybutyrate dehydrogenase in the liver, while itaconate (Itac) limits mitochondrial substrate-level phosphorylation as it is a preferred substrate for succinate-CoA ligase, which also leads to a CoASH-trap [28], thus exerting metabolic pressure on the overall citric acid cycle. The increases in OXPHOS capacities were not merely additive but strongly synergistic to that conferred by succinate in liver (Figure 1F,G) and kidney mitochondria (Figure 1K,L). OXPHOS capacity with the succinate and proline substrate combination (J_{SPro}) was 1.4- and 1.2-fold higher than the arithmetic sum $J_{Pro} + J_S$ (Table 1), thereby demonstrating a synergistic effect and excess additivity [29]. In contrast, additivity in the LEAK state was partially or completely additive in liver mitochondria. In kidney mitochondria, additivity was even negative in the LEAK state, indicating suppression of LEAK respiration when proline was added to succinate (Table 1; Supplementary Table S1).

Table 1. Additivity of convergent succinate and proline pathway OXPHOS capacity in liver and kidney mitochondria. Median additivity >1 indicates 'excess additivity' and synergistic activation of O_2 flux, when flux of the combined pathway J_{SPro} is higher than the arithmetic sum of fluxes for the individual pathways J_{Pro}+J_S. Negative additivity indicates suppression of flux in the presence of the substrate combination [29].

	Proline	Succinate	J_{Pro}/J_{SPro}	J_S/J_{SPro}	Additivity
	[mM]	[mM]			
Liver OXPHOS	2	5	0.30	0.40	2.04
	5	5	0.30	0.41	1.95
Liver LEAK	2	5	0.55	0.67	0.59
	5	5	0.40	0.59	1.03
Kidney OXPHOS	2	5	0.19	0.60	2.11
	5	5	0.26	0.58	1.62
Kidney LEAK	2	5	0.25	1.10	−0.39
	5	5	0.39	1.08	−0.20

2.3. Effect of Proline on ΔΨmt, NADH Autofluorescence and Q Redox State of Isolated Mitochondria

Being mindful that, in the presence of NADH-linked substrates (glutamate, malate, βOH), the addition of proline did not yield an additional increase in the oxygen consumption rate, we questioned whether this was because of the downstream production of glutamate (see Scheme 1) that would fuel the citric acid cycle or be a limitation of the measurement itself—having saturated the capacity of CIV transferring electrons to molecular oxygen. Therefore, we examined the effects of proline on other bioenergetic readouts, namely $\Delta\Psi_{mt}$, NADH autofluorescence, and the Q redox state of isolated mitochondria. As shown in Figure 2A for liver and Supplementary Figure S1A for kidney, mitochondria

were added in the buffer without substrates and allowed to develop a transient membrane potential before exhibiting a depletion of endogenous substrates, thereby leading to a complete loss of $\Delta\Psi_{mt}$. Subsequently, proline was added in boluses at the concentrations indicated in the panels, thereby leading to progressive polarization. The further addition of glutamate (G) and malate (M) did not yield any further increase in $\Delta\Psi_{mt}$. On the other hand, the addition of succinate (S; Figure 2B for liver and Figure S1B for kidney mitochondria) led to a further decrease in safranine O fluorescence, which is indicative of a gain in $\Delta\Psi_{mt}$—even in the presence of rotenone. Importantly, the presence of rotenone did not abolish the proline-induced polarization. However, the CIII inhibitor, myxothiazol, completely inhibited the proline-induced polarization in both liver (Figure 2D) and kidney (Figure S1C) mitochondria. On the other hand, atpenin A5 blocked the succinate-induced gain in $\Delta\Psi_{mt}$, but the proline-induced changes remained unaffected (Figure 2C for liver mitochondria).

In congruence with the data showing $\Delta\Psi_{mt}$, additions of proline to mitochondria led to a dose-dependent increase in NADH autofluorescence; NADH autofluorescence was recorded fluorometrically using two different equipment: a Hitachi F-7000 fluorescence spectrophotometer or an Oroboros NextGen-O2k. Data obtained with the Hitachi are shown in Figure 2E (for liver mitochondria) and Figure S1D (for kidney mitochondria), while those obtained with the NextGen-O2k are shown in Figure 2G (for liver mitochondria) and Figure S3B (for kidney mitochondria). The oxygen consumption rate, NADH autofluorescence, and rhodamine 123 fluorescence (indicative of $\Delta\Psi_{mt}$) were simultaneously recorded and shown in Figure 2F–H, respectively, for the liver, and Figure S3A–C for the kidney, which are aligned on the dashed grey lines using the NextGen-O2k. As shown in Figure 2E,G, Figures S1D and S3B, the subsequent addition of rotenone led to greater increases in NADH autofluorescence depending on the amount of proline added to mitochondria. This additional increase in NADH depending on the proline concentration reflects the NADH originating from the reaction catalyzed by ALDH4A1, which is upstream of glutamate (see Scheme 1).

To strengthen the above conclusions that proline is catabolized in liver and kidney mitochondria, we recorded the quinone (Q) redox state using an Oroboros NextGen-O2k, which was measured simultaneously with the oxygen consumption rate and rhodamine 123 fluorescence (indicative of $\Delta\Psi_{mt}$). As shown in Figure 3A–C (for liver mitochondria) and Figure S2A–C (for kidney mitochondria), bolus additions of proline (concentrations indicated in the panels) led to measurable increases in oxygen consumption rates, Q reduction, and gains in $\Delta\Psi_{mt}$. The increases in Q reduction were less pronounced in the presence of rotenone (Figure 3E for liver and Figure S2E for kidney mitochondria) than in the absence of this CI inhibitor (Figure 3B and Figure S2B for liver and kidney mitochondria, respectively). The 'dampening' of changes in the Q reduction in the presence of rotenone (which is expected to lead to an increase in matrix NADH/NAD^+) reflect the part of proline catabolism that is downstream from ProDH, specifically the NAD^+-requiring ALDH4A1, GDH, and OgDH steps; they probably signal an increase of substrate(s), leading to a moderate decrease in ProDH activity and yielding the less-pronounced effect of proline on the Q redox state in the presence of rotenone. The changes in Q reduction are shown as a non-calibrated signal; thus, at the end of the experiments, succinate was added and was followed by SF6847. This was done in order to provide a semi-quantitative estimation of the Q reduction by proline compared to the reduction by succinate dehydrogenase and the oxidation of the electron transfer system (ETS) due to the uncoupler. As expected, in the presence of CIII inhibitor and myxothiazol, proline led to no changes in the Q reduction state (Figure 3H), which was monitored simultaneously with the oxygen consumption rate (Figure 3G) and rhodamine 123 fluorescence (Figure 3I).

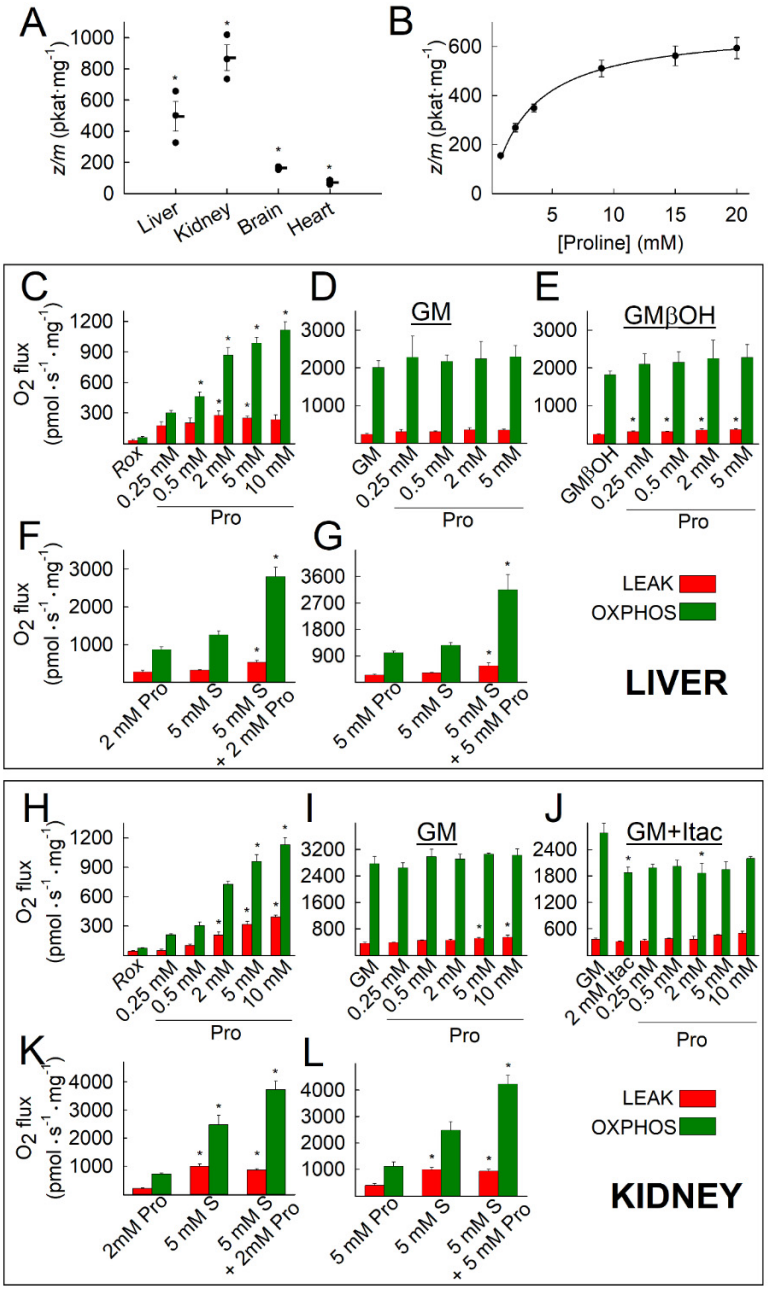

Figure 1. Kinetic characterization of ProDH activity in isolated mitochondria (**A**,**B**), and the effect of proline concentration on oxygen consumption rates (LEAK: red bars; OXPHOS: green bars) of isolated mouse liver (**C**–**G**) and kidney (**H**–**L**) mitochondria using various substrate combinations and concentrations. (A) ProDH catalytic activity content (expressed in pkat/mg) of mitochondria isolated from mouse liver, kidney, brain, and heart using saturating concentrations of proline (100 mM) * $p < 0.05$ (comparing all groups with each other; ANOVA on Ranks). Data are SEM averaged from three independent experiments. (**B**) Determination of apparent K_m of mouse liver ProDH for proline. Data points are SEM averaged from three independent experiments. (**C**,**H**) Rox: residual oxygen consumption (no external substrate added; increased OXPHOS indicates the effect of ADP stimulating respiration on internal substrates), followed by proline titrations. (**D**,**I**) GM: glutamate and malate, followed by proline titrations. (**E**) GM and 2 mM βOH, followed by proline titration. (**J**) GM: glutamate and malate, 2 mM Itac: GM+2 mM itaconate, followed by proline titration. (**F**,**K**,**G**,**L**) Proline (Pro) and/or succinate (S). Data are SEM averaged from at least three independent experiments. For C–L, * $p < 0.05$ (ANOVA Bonferroni [comparisons are to controls, i.e., no proline] or on ranks, if normality failed).

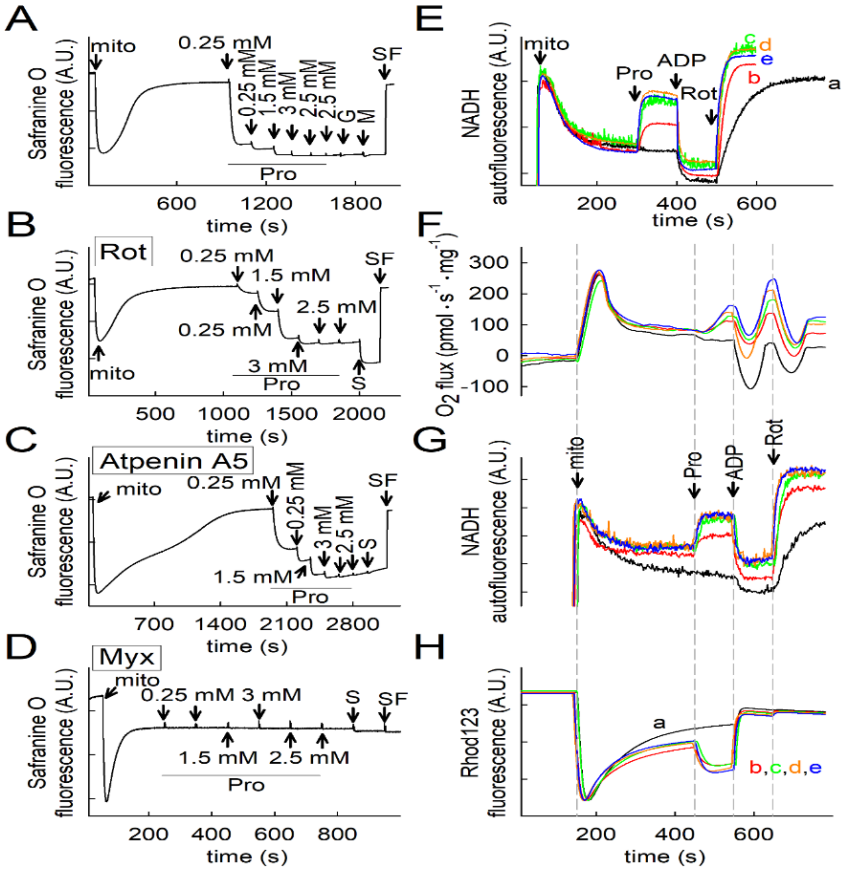

Figure 2. Effect of proline concentration on $\Delta\Psi_{mt}$ and NADH autofluorescence of isolated mouse liver mitochondria subjected to targeted inhibition of electron transfer (ET) pathways. No substrates were present prior to the addition of mitochondria. Glutamate (G), malate (M), and proline (Pro) were added at concentrations indicated. (**A**–**D**) Time course of safranine O signal indicative of $\Delta\Psi_{mt}$ (arbitrary units, A.U.). SF6847 (SF, 1 μM). (**A**) No targeted inhibition of electron transfer pathways. (**B**) 1 μM rotenone (Rot) present in the buffer prior to addition of mitochondria; succinate (S, 5 mM). (**C**) As in B, but 1 μM atpenin A5 replaced Rot. (**D**) As in B, but myxothiazol (Myx) replaced Rot. (**E**–**H**) Concentrations of Pro: black (a): 0 mM, red (b): 0.25 mM, green (c): 0.5 mM, orange (d): 2 mM, blue (e): 5 mM. (**E**) NADH autofluorescence (arbitrary units A.U.) measured in the Hitachi F-7000 fluorescence spectrophotometer. (**F**–**H**) Oxygen consumption, NADH autofluorescence, and rhodamine 123 fluorescence indicative of $\Delta\Psi_{mt}$ (arbitrary units A.U.), respectively, recorded simultaneously from the same liver mitochondria using the NextGen-O2k and aligned on the dashed grey lines.

In accordance with the lower ProDH activities measured in brain and heart mitochondria (Figure 1A), the addition of proline to brain (Figure S4A) or heart (Figure S4C) mitochondria led to a moderate gain of $\Delta\Psi_{mt}$. Accordingly, while measuring NADH autofluorescence or Q reduction, the addition of proline to brain or heart mitochondria led to evanescent changes—as shown in Figure S4B,D for NADH autofluorescence in brain and heart mitochondria and Figure S4F for the Q redox state in brain mitochondria, which was measured simultaneously with the oxygen consumption rate (Figure S4E) and rhodamine 123 fluorescence (Figure S4G).

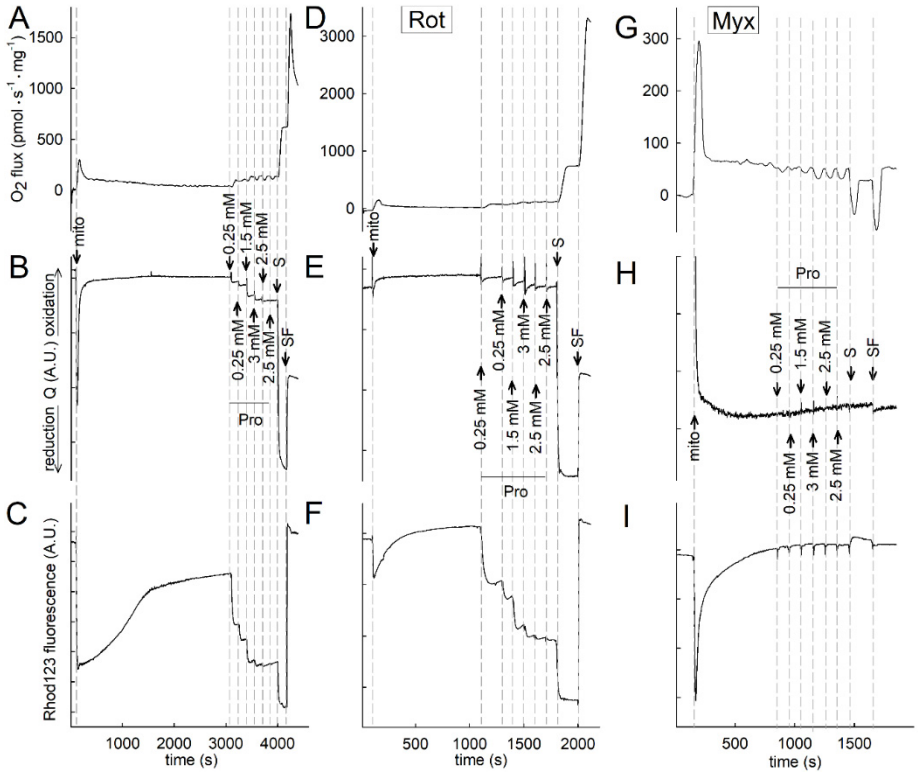

Figure 3. Coenzyme Q (Q) redox state recorded simultaneously with oxygen consumption rate and rhodamine 123 fluorescence in isolated mouse liver mitochondria using the NextGen-O2k. (**A**) Oxygen consumption. (**B**) Q redox state. (**C**) Rhodamine 123 fluorescence indicative of $\Delta\Psi_{mt}$ (arbitrary units A.U.). No substrates were present. Succinate (S, 5 mM) and proline (Pro) were added at the concentrations indicated. 0.25 µM SF (**D**–**F**) as in A, B, and C, but rotenone was present in the medium. (**G**–**I**) As in A, B, and C, but 0.1 µM myxothiazol was present in the medium.

2.4. Proline Oxidation Is Sensitive to Tetrahydro-2-Furoic Acid (THFA) and S-5-Oxo-2-Tetrahydrofurancarboxylic Acid (S-5-oxo)

Tetrahydro-2-furoic acid (THFA) and S-5-oxo-2-tetrahydrofurancarboxylic acid (S-5-oxo) have been described as specific inhibitors of ProDH, the latter compound branded as a "second-generation" from the former [30,31]. In our hands, 10 mM THFA inhibited the ProDH activity of liver and kidney mitochondria to a great extent (>80 % inhibition, see Figure 4A), while S-5-oxo had little—if any—effect at 5 mM. THFA exhibited a dose-dependent decrease in LEAK and OXPHOS respiration in both liver (Figure 4B) and kidney (Figure 4D) mitochondria. At 10 mM, S-5-oxo only inhibited proline oxidation in liver (Figure 4C), but not kidney (Figure 4E), mitochondria.

2.5. Effect of Proline Dehydrogenase Inhibitors on Proline-Induced Changes in Q Redox State and ΔΨmt

Based on the inhibitory effects of THFA and S-5-oxo on ProDH activity and proline-mediated respiration, we sought to establish the effect of these inhibitors on other proline-mediated bioenergetic read-outs. For this, we investigated the effects of the compounds on proline-induced changes in the Q redox state and $\Delta\Psi_{mt}$. As shown in Figure 4, liver mitochondria THFA and S-5-oxo abolished the proline-induced Q reduction (proline added after ADP and the CI inhibitor rotenone) and decreased rhodamine 123 fluorescence, which is indicative of $\Delta\Psi_{mt}$. The Q redox state and rhodamine fluorescence were recorded simultaneously with oxygen consumption and were aligned on the dashed grey lines. The results obtained from THFA are shown in Figure 4F–H, and for S-5-oxo they are shown in Figure 4I–K. Various traces imply different substrate combinations and different concentrations of the ProDH inhibitor, which are detailed in the legend. Qualitatively

similar results were obtained from kidney mitochondria, which are shown in Figure S5. In Figure S5A, the dose-dependent effect of THFA was examined for the proline-induced changes of safranine O fluorescence, which is indicative of $\Delta\Psi_{mt}$, while in Figure S5B–D, they were recorded simultaneously using a NextGen-O2k (aligned in the grey dashed lines). The effects of THFA on respiration, the Q redox state, and rhodamine 123 fluorescence are shown. Various traces imply different substrate combinations and different concentrations of the ProDH inhibitor, which are detailed in the legend.

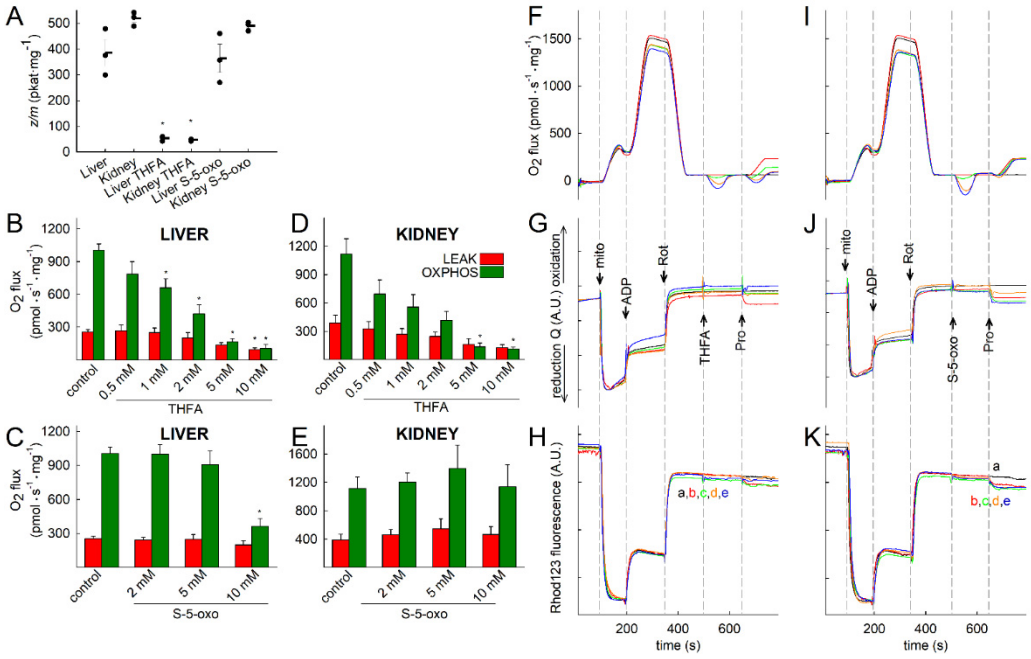

Figure 4. The effects of THFA and S-5-oxo on ProDH activity (**A**), on proline—mediated respiration rates in isolated mouse liver and kidney mitochondria (* p <0.05 ANOVA on Ranks (Liver) or Bonferroni (Kidney; comparisons are to controls, i.e., no proline or no ProDH inhibitor added)); (**B**–**E**), and on oxygen consumption, Q redox state, and rhodamine 123 fluorescence, which were recorded simultaneously from liver mitochondria using the NextGen-O2k (**F**–**K**). (A) Scatter plot depicting ProDH catalytic activity (pkat/mg protein of isolated mitochondria) with 10 mM proline and the effects of THFA (10 mM) and S-5-oxo (5 mM). (**B**) Bar graph depicting LEAK (red) and OXPHOS (green) oxygen consumption rates in liver mitochondria respiring on 5 mM proline as a function of THFA concentration. (**C**) As in B but using S-5-oxo instead of THFA. (**D**) As in B but with kidney mitochondria. (**E**) As in C but with kidney mitochondria. Data are SEM of at least three independent experiments. (**F**–**K**) Proline (Pro, 5 mM), (**F**–**H**) THFA, (**I**–**K**) S-5-oxo. GMβOH always present: glutamate (G), malate (M), and βOH (10 mM). Black (a): GMβOH; red (b): plus proline (Pro, 5 mM); green (c): plus Pro and THFA (2 mM) or S-5-oxo (2 mM); orange (d): plus Pro and THFA (5 mM) or S-5-oxo (5 mM); blue (e): plus Pro and THFA (10 mM) or S-5-oxo (10 mM). For B–E, * p <0.05 ANOVA (Bonferroni or on ranks).

2.6. Effect of Proline on ANT Directionality

From the above experiments, it is evident that mouse liver and kidney (and to a much lesser extent brain and heart) mitochondria, and in accordance with the corresponding ProDH activities, proline is catabolized and generates $\Delta\Psi_{mt}$ in a manner that is dependent on CIII (and CIV) function. In order to address if this is sufficient for maintaining matrix ATP levels, we interrogated the directionality of ANT, a parameter that is profoundly sensitive to matrix [ATP]/[ADP] [18,32,33]. ANT directionality was addressed using a biosensor test developed by us, in which the effect of the ANT inhibitor carboxyatractyloside (CAT) is examined for $\Delta\Psi_{mt}$ during ADP-induced respiration but after targeted inhibition of the ETS [32]. Briefly, the adenine nucleotide exchange through the ANT is

electrogenic, since one molecule of ATP^{4-} is exchanged for one molecule of ADP^{3-} [34]. In fully energized mitochondria, the export of ATP in exchange for ADP costs ~25% of the total energy produced [35]. Therefore, during the forward mode of ANT, the abolition of its operation by CAT leads to a gain of $\Delta\Psi_{mt}$, whereas during the reverse mode of ANT, the abolition of its operation by the inhibitor leads to $\Delta\Psi_{mt}$ loss.

A generalized scheme is depicted in [36]. As shown in Figure 5, mouse liver mitochondria proline kept the ANT operating in its forward mode irrespective of the substrate combinations used and indicated if it was present before or after ETS inhibition by rotenone (Figure 5A–D).

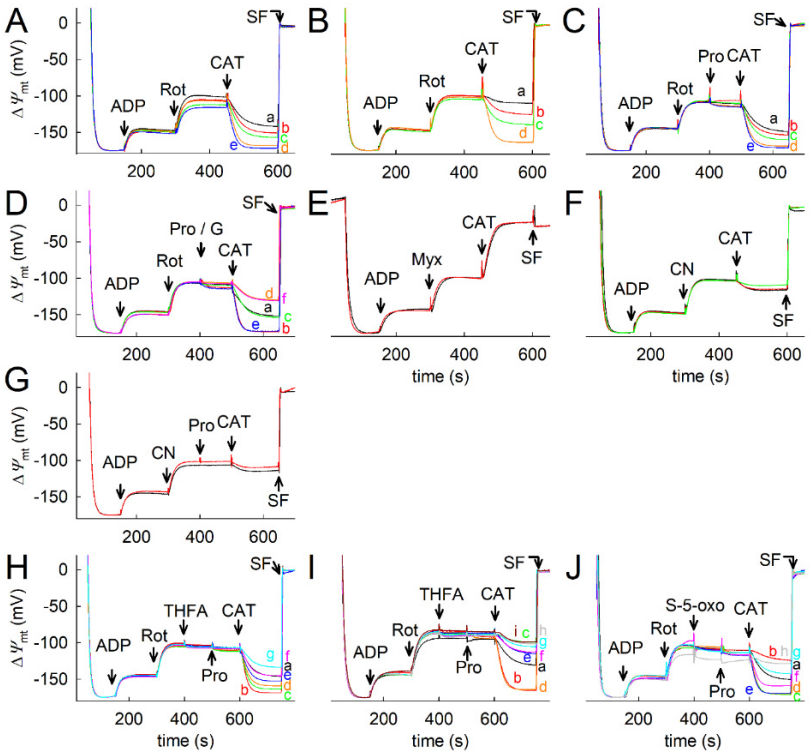

Figure 5. The effect of proline on ANT directionality (**A**–**G**), and the effect of THFA and S-5-oxo on proline-induced changes of ANT directionality (**H**–**J**) in isolated mouse liver mitochondria as a function of the targeted inhibition of electron transfer pathways using various substrate–inhibitor combinations. Traces are time courses of the safranine O signal calibrated to $\Delta\Psi_{mt}$. (**A**) GM is always present for increasing concentrations of proline (Pro); black (a): 0 mM; red (b): 0.25 mM; green (c): 0.5 mM; orange (d): 2 mM; blue (e): 5 mM. (**B**) As in A, but GM and 5 mM βOH always present. (**C**) As in A, but proline added after rotenone. (**D**) Black (a): GM; red (b): GM plus 5 mM Pro; green (c): GM plus additional 5 mM glutamate added where indicated; orange (d): GMβOH; blue (e): GMβOH plus 5 mM Pro added where indicated; magenta (f): GM and 5 mM βOH plus additional 5 mM glutamate added where indicated. (**E**) Black: GM; red: GM and 5 mM Pro. (**F**) black: GM; red: GM and 2 mM Pro; green: GM and 5 mM Pro; NaCN (CN, 1 mM) added where indicated. (**G**) black: GM; red: GM and 5 mM proline added after NaCN (CN, 1 mM). (**H**–**J**) GM always contained in the medium. GMPro contains 5 mM proline. GMβOH contains 5 mM βOH, GMProβOH containes 5 mM Pro and 5 mM βOH. (**H**) Black (a): GM; red (b): GMPro; green (c): GMPro and 1 mM THFA; orange (d): GMPro and 2 mM THFA; blue (e): GMPro and 5 mM THFA; magenta (f): GMPro and 10 mM THFA; cyan (g): GM and 10 mM THFA. (**I**) Black (a): GM; red (b): GMPro; green (c): GMβOH; orange (d): GMProβOH; blue (e): GMProβOH and 10 mM THFA; magenta (f): GMProβOH and 15 mM THFA; cyan (g): GMProβOH and 20 mM THFA; grey (h): GMProβOH and 25 mM THFA; brown (i): GM and 25 mM THFA. (**J**) Black (a): GM; red (b): GMβOH; green (c): GMPro; orange (d): GMProβOH; blue (e): GMProβOH and 10 mM S-5-oxo; magenta (f): GMProβOH and 15 mM S-5-oxo; cyan (g): GM and 10 mM S-5-oxo; grey (h): GM and 15 mM S-5-oxo.

However, when ETS was blocked at the level of CIII with myxothiazol (Myx, 5E) or CIV with cyanide (CN, 5F,G), proline failed to maintain the ANT in forward mode, implying that any changes conferred by proline required the uninterrupted operation of both CIII and CIV. Importantly, an excess of glutamate could not reproduce the effects of proline (Figure 5D), thereby indicating that the effects of proline are not due to the downstream formation of glutamate. As expected, the effects of proline in liver mitochondrial ANT directionality were sensitive to inhibition by both THFA (Figure 5H,I) and S-5-oxo (Figure 5J). Qualitatively similar results were obtained with kidney (Figures S6 and S7), brain (Figure S8), and heart (Figure S9) mitochondria, which were always in accordance with ProDH activities; however, S-5-oxo was much less potent than THFA in kidney mitochondria. In experiments using kidney mitochondria, 2-ketobutyrate was also included; 2-ketobutyrate negates mSLP due to the ATP-consuming propionyl-CoA carboxylase step [37], and this was used as a way to limit mSLP and examine any beneficial effects of proline that could be affected by the ProDH inhibitors. As was also expected, proline had no effect on the ANT directionality of mitochondria subject to anoxia (i.e., complete non-pharmacological CIV inhibition)—as shown in Figure 6. Interestingly, proline exhibited a dose-dependent effect in CAT-induced Q reduction in the presence of glutamate and malate (Figure 7B), which was dampened if βOH was concomitantly present (Figure 7E). These recordings were simultaneously measured with the oxygen consumption rate and rhodamine 123 fluorescence (indicative of $\Delta\Psi_{mt}$) (Figure 7A,D and Figure 7C,F, respectively) using the NextGen-O2k in isolated liver mitochondria. Qualitatively similar results were obtained with kidney mitochondria (Figure S10). The reason(s) for the CAT-induced changes in the Q redox state during CI inhibition, and as a function of proline, were not investigated further. As expected, when CIII was inhibited by myxothiazol (Figure 8A–C) or under anoxia (Figure 8D–F), these phenomena were not observed. Qualitatively similar results were obtained with anoxic (Figure S11) and CIII-inhibited kidney mitochondria (Figure S10E).

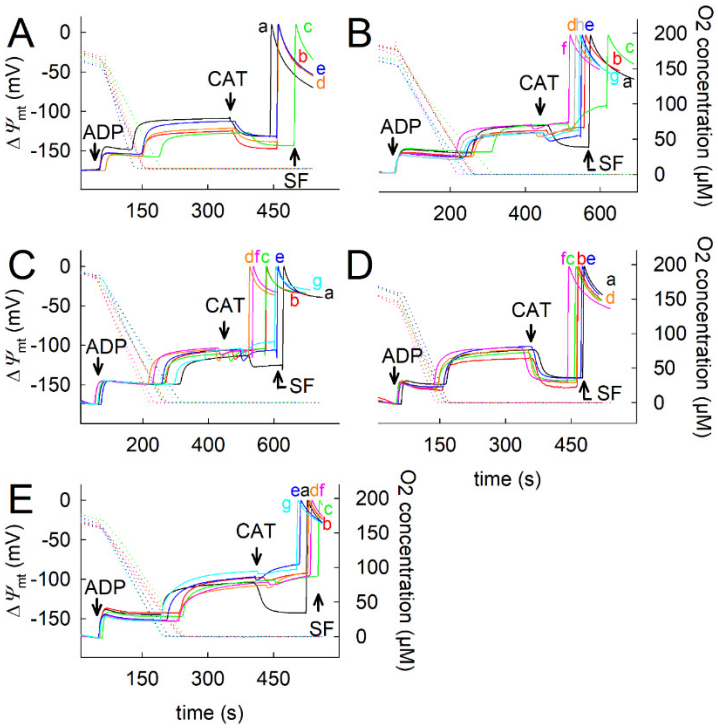

Figure 6. Lack of effect of proline on ANT in anoxic mouse liver (**A**–**C**) and kidney (**D**,**E**) mitochondria. Traces are time courses of simultaneous measurements of safranine O signal calibrated to $\Delta\Psi_{mt}$ (solid lines) and oxygen concentration in the media (dotted lines). GM always contained in the medium. (**A**) GM and increasing concentrations of Pro; black (a): 0 mM; red (b): 0.25 mM; green (c): 0.5 mM; orange (d): 2 mM; blue (e): 5 mM. (**B**) GM or GM and itaconate (1 mM or 2 mM in traces b to h), as

well as increasing concentrations of Pro; black (a): 0 mM; red (b): 1 mM itaconate and 0 mM; green (c): 2 mM itaconate and 0 mM; orange (d): 1 mM itaconate and 0.25 mM; blue (e): 1 mM itaconate and 0.5 mM; magenta (f): 1 mM itaconate and 2 mM; cyan (g): 1 mM itaconate and 5 mM; grey (h): 1 mM itaconate and 10 mM. (**C**) GM or GM and βOH in traces b to g and increasing concentrations of Pro; black (a): 0 mM; red (b): 0 mM; green (c): 0.25 mM; orange (d): 0.5 mM; blue (e): 2 mM; magenta (f): 5 mM; cyan (g): 10 mM. (**D**) GM and increasing concentrations of Pro; black (a): 0 mM; red (b): 0.25 mM; green (c): 0.5 mM; orange (d): 2 mM; blue (e): 5 mM; magenta (f): 10 mM. (**E**) GM (a) or GM and itaconate in traces b to g, as well as increasing concentrations of Pro; black (a): 0 mM; red (b): 0 mM; green (c): 0.25 mM; orange (d): 0.5 mM; blue (e): 2 mM; magenta (f): 5 mM; cyan (g): 10 mM.

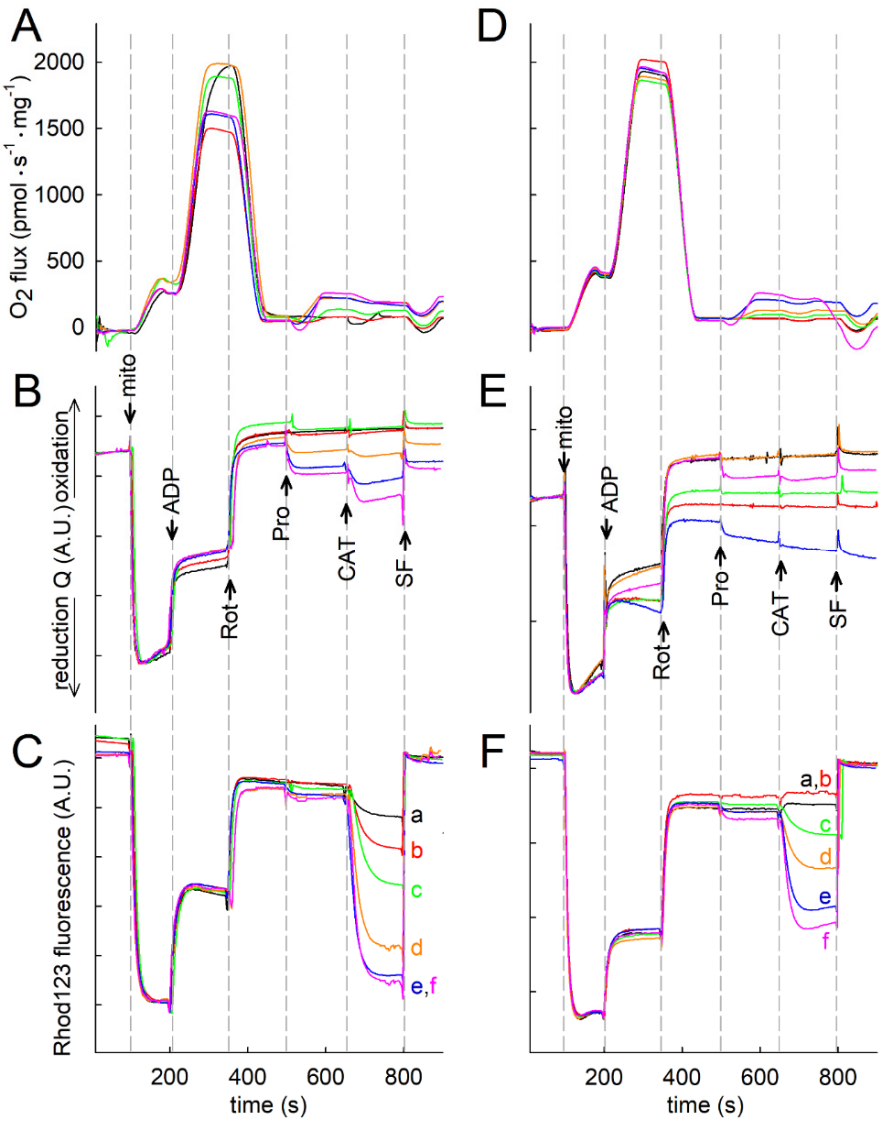

Figure 7. The effect of proline on CAT-induced changes in respiration (**A**,**D**), Q redox state (**B**,**E**), and rhodamine 123 fluorescence (**C**,**F**), which are indicative of $\Delta\Psi_{mt}$ (arbitrary units A.U.) and were measured simultaneously in the same mouse liver mitochondria using the NextGen-O2k—aligned on the dashed grey lines. GM was always contained in the medium; 0.25 µM SF. (**A**–**C**) GM and increasing concentrations of Pro; black (a): 0 mM; red (b): 0.25 mM; green (c): 0.5 mM; orange (d): 2 mM; blue (e): 5 mM; magenta (f): 10 mM. (**D**–**F**) 5 mM βOH is additionally present in traces b–f and increasing concentrations of Pro; black (a): 0 mM; red (b): 0 mM; green (c): 0.25 mM; orange (d): 0.5 mM; blue (e): 2 mM; magenta (f): 5 mM.

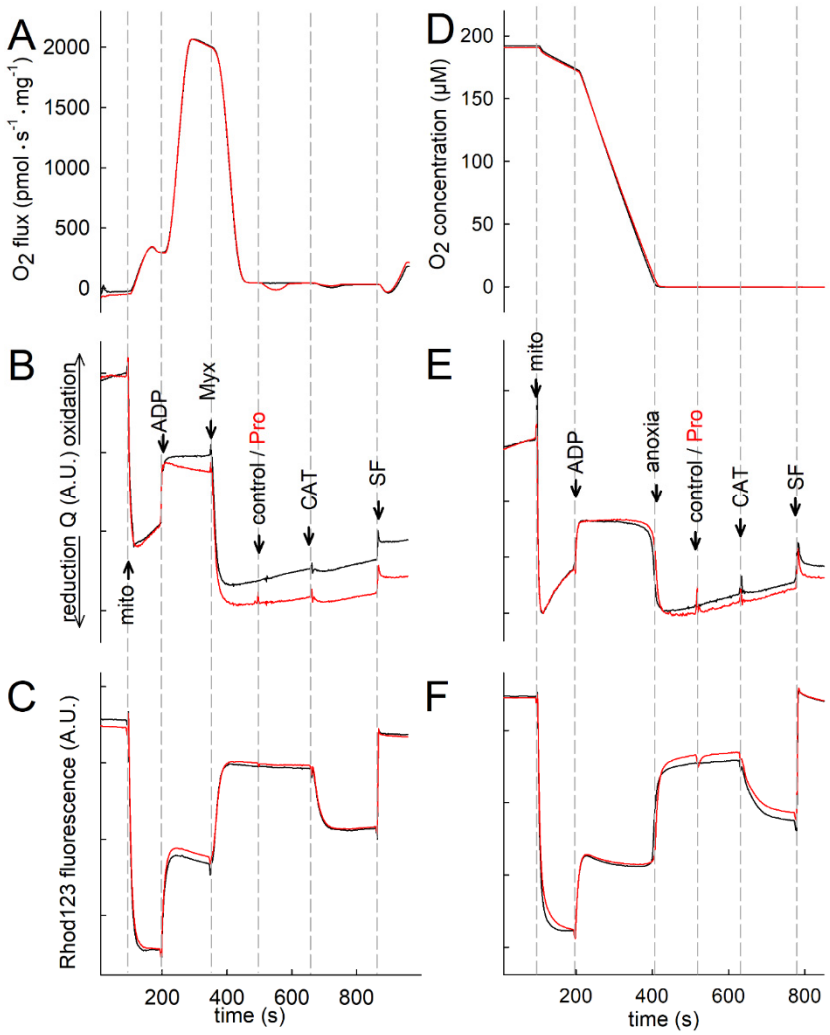

Figure 8. No effect of proline on Q redox state of mitochondria inhibited at CIII (myxothiazol, 0.1 µM) or under anoxia. Oxygen consumption (**A**) or concentration (**D**), Q redox state (**B**,**E**), and rhodamine 123 fluorescence (**C**,**F**) are indicative of $\Delta\Psi_{mt}$ (arbitrary units A.U.) and were measured simultaneously in the same mouse liver mitochondria using the NextGen-O2k—aligned on the dashed grey lines. Black traces: GM (and 10 mM βOH in **D**–**F**); red trace: GM plus 5 mM proline where indicated (& 10 mM βOH in **D**–**F**). 0.25 µM SF.

2.7. Proline Oxidation Maintains F_1F_O-ATPase in Forward Mode during Complex I Inhibition

When mitochondria depend on pyruvate or other widely used NADH-linked substrates, such as glutamate or oxoglutarate, to support respiration, inhibition of the electron transport system at the level of CI leads to F_1F_O-ATPase reversal [38,39]. This results in the maintenance of a $\Delta\Psi_{mt}$ value that is no higher than the reversal potential of the F_1F_O-ATPase [18,33]. Being mindful that proline fuels mitochondria through ProDH reducing Q reminiscent of CI bypass [40–42], we sought to address the directionality of the F_1F_O-ATPase in mitochondria supported by proline in the presence of the CI inhibitor rotenone. This was done in a manner similar to interrogating the ANT directionality but using the F_1F_O-ATPase inhibitor oligomycin (Omy) instead of CAT. As shown in Figure 9 for liver and Figure S12 for kidney mitochondria, proline added in various concentrations, as indicated in the legends, maintained F_1F_O-ATPase in the forward mode; this was not observed if CIII was inhibited by myxothiazol (Myx, 9E, S12F) or if CIV was inhibited by cyanide (CN, 9F, S12G).

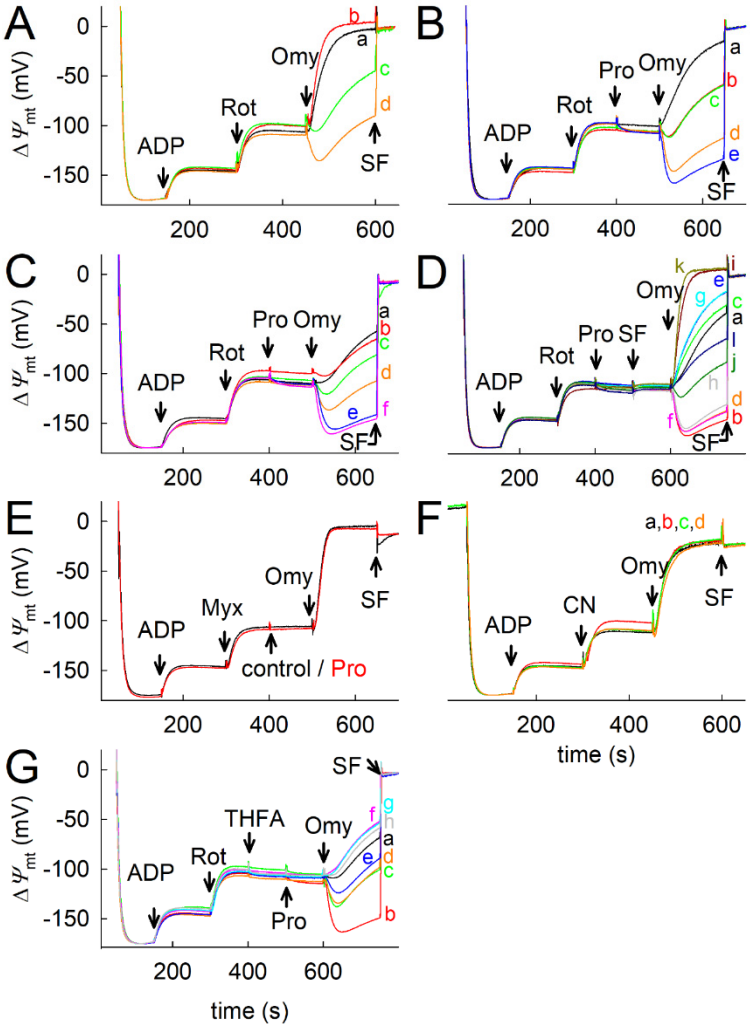

Figure 9. The effect of proline on F_1F_O-ATPase directionality in isolated mouse liver mitochondria as a function of the targeted inhibition of electron transfer pathways using various substrate–inhibitor combinations. Traces are time courses of safranine O signal calibrated to $\Delta\Psi_{mt}$. (**A**) GM and increasing concentrations of Pro were always contained in the medium; black (a): 0 mM; red (b): 0.5 mM; green (c): 1 mM; orange (d): 2 mM. (**B**) GM and increasing concentrations of Pro were added where indicated; black (a): 0 mM; red (b): 0.25 mM; green (c): 0.5 mM; orange (d): 2 mM; blue (e): 5 mM. (**C**) As in B, but in traces b-f there is 15 mM βOH additionally present; black (a): 0 mM; red (b): 0 mM; green (c): 0.25 mM; orange (d): 0.5 mM; blue (e): 2 mM; magenta (f): 5 mM. (**D**) Black (a): GM; red (b): GM and 5 mM Pro; green (c): GM and 1 nM SF added @500 s; orange (d): GM and 1 nM SF added @500 s and 5 mM Pro; blue (e): GM and 2 nM SF added @500 s; magenta (f): GM and 2 nM SF added @500 s and 5 mM Pro; cyan (g): GM and 3 nM SF added @500 s; grey (h): GM and 3 nM SF added @500 s and 5 mM Pro; brown (i): GM and 4 nM SF added @500 s; dark green (j): GM and 4 nM SF added @500 s and 5 mM Pro; dark yellow (k): GM and 5 nM SF added @500 s; dark blue (l): GM and 5 nM SF added @500 s and 5 mM Pro. (**E**) Myxothiazol (Myx); black trace: GM; red trace: GM and 5 mM Pro. (**F**) NaCN (CN); black (a): GM; red (b): GM and 0.5 mM Pro; green (c): GM and 1 mM Pro; orange (d): GM and 2 mM Pro. (**G**) Black (a): GM; red (b): GM and 5 mM Pro; green (c): GM and 2 mM THFA and 5 mM Pro; orange (d): GM and 5 mM THFA and 5 mM Pro; blue (e): GM and 10 mM THFA and 5 mM Pro; magenta (f): GM and 2 mM THFA; cyan (g): GM and 5 mM THFA; grey (h): GM and 10 mM THFA.

In agreement with the data above, THFA (9G, S12C, S12D) could abolish the proline effect. Importantly, the effect of proline maintaining F_1F_O-ATPase operation in the forward mode was primarily due to a small but sufficient gain in $\Delta\Psi_{mt}$, which effectively crossed

the reversal potential of the F_1F_O-ATPase "to the left"—see [36]. This was deduced from the experiments shown in Figure 9D for liver and Figure S12E for kidney mitochondria. In these experiments, the uncoupler SF6847 was titrated to clamp $\Delta\Psi_{mt}$ to a level that was equal to just before proline addition. Indeed, at these SF6847 concentrations, the effect of proline was abolished. From this, we concluded that proline was maintaining F_1F_O-ATPase in the forward mode exclusively because of a gain in $\Delta\Psi_{mt}$ due to proton pumping by CIII and CIV, which is supported by the Q reduction through ProDH.

Finally, proline exerted an effect on the oligomycin-induced Q reduction in the presence of glutamate and malate (Figure S13B), just like CAT (Figure 7B). These recordings were simultaneously made with the oxygen consumption rate and rhodamine 123 fluorescence (indicative of $\Delta\Psi_{mt}$) (Figures S13A and S13C, respectively) using the NextGen-O2k. The reason(s) for the oligomycin-induced changes in the Q redox state during CI inhibition as a function of proline were not investigated further.

2.8. Fueling Complex III with Duroquinone Only Partially Mimics the Benefits of Proline

As shown from the results above, proline is oxidized by ProDH reducing Q, which is in turn oxidized by CIII and also requires CIV and oxygen as a final electron acceptor. Thus, we sought to compare the effects of proline with duroquinone (DQ), an artificial substrate of CIII. As shown in Figure 10A (for liver) and 10B (for kidney), DQ could partially mimic the effect of proline in maintaining F_1F_O-ATPase in the forward mode. Higher concentrations of DQ had deleterious effects, as they probably damage the mitochondrial inner membrane. Thus, proline is a far superior substrate for fueling CIII—though indirectly through Q. Furthermore, the effects of proline could not be reproduced by ornithine (Figure 10C), a metabolite forming GSA by transamination with Og (see Scheme 1); being mindful that GSA is downstream to proline oxidation by ProDH, it is concluded that proline effects are exclusively due to upstream Q reduction. In addition, proline could also partially rescue ANT and F_1F_O-ATPase operation reversal induced by arsenite ($NaAsO_2$)—an inhibitor of dehydrogenases including oxoglutarate dehydrogenase (Figure 10D)—thus its effects are unrelated to the dehydrogenase. Finally, the effects of proline were unaffected by dicoumarol, thus they are not mediated through diaphorases (Figure 10E).

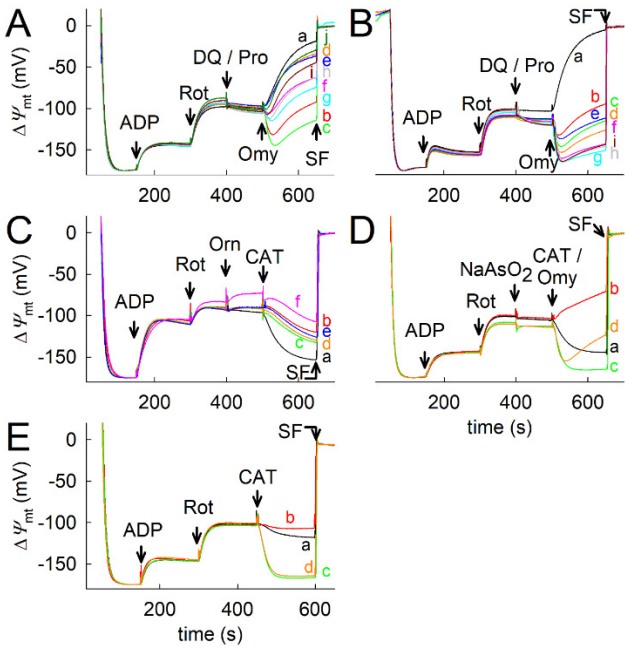

Figure 10. Fuelling of CIII with duroquinone (DQ), but not ornithine, partially mimics the effects of proline; neither arsenite nor dicoumarol antagonize proline. Traces are time courses of safranine O signal calibrated to $\Delta\Psi_{mt}$. 0.25 µM SF. (**A**) Liver mitochondria; GM always present and the following

additions; black (a): no other additions; red (b): 2 mM Pro; green (c): 5 mM Pro; orange (d): 0.01 mM duroquinone (DQ); blue (e): 0.05 mM DQ; magenta (f): 0.1 mM DQ; cyan (g): 0.2 mM DQ; grey (h): 0.3 mM DQ; brown (i): 0.4 mM DQ; dark green (j): 0.5 mM DQ. (**B**) kidney mitochondria; GM always present and the following additions; black (a): no other additions; red (b): 2 mM Pro; green (c): 5 mM Pro; orange (d): 10 mM Pro; blue (e): 0.01 mM DQ; magenta (f): 0.05 mM DQ; cyan (g): 0.1 mM DQ; grey (h): 0.2 mM DQ; brown (i): 0.3 mM DQ. (**C**) Liver mitochondria; 5 mM oxoglutarate (Og) always present and the following additions; black (a): no other additions; red (b): 2 mM ornithine (Orn); green (c): 5 mM Orn; orange (d): 10 mM Orn; blue (e): 20 mM Orn; magenta (f): 40 mM Orn. (**D**) Liver mitochondria; GM always present and the following additions; black (a): no other additions; red (b): 2 mM $NaAsO_2$; green (c): 5 mM Pro and 2 mM $NaAsO_2$; orange (d): 5 mM Pro and 2 mM NaA_SO_2. (**E**) Liver mitochondria. GM & 5 mM βOH always present and the following additions; black (a): no other additions; red (b): 0.5 µM dicoumarol; green (c): 5 mM proline; orange (d): 5 mM proline & 0.5 µM dicoumarol.

3. Discussion

It is a textbook definition that the F_1F_O-ATPase reverses, pumping protons out of the matrix even at the cost of ATP consumption, thereby preserving the mitochondrial membrane potential when CI is inhibited, and only NADH-linked substrates are available [29,38,39]. The most important conclusion of the present study is that the above statement does not apply when mitochondria oxidize proline through ProDH. We showed that, in CI-inhibited mitochondria exhibiting a sufficiently high ProDH activity, the reduction of ubiquinone fueling CIII and CIV, which leads to proton pumping, supports $\Delta\Psi_{mt}$ to a level at which the F_1F_O-ATPase maintains ATP production. This finding agrees with a modelling study in which the authors claimed that CI deficiency was maybe compensated for by proline oxidation [43].

Notably, this property of proline is not due to catabolism towards glutamate and oxoglutarate, as further catabolism of either metabolite requires CI activity. However, the effect of proline on the Q redox state was partially sensitive to rotenone, implying the continuity of the pathway Pro -> P5C -> GSA -> G -> Og, where the first step generates reduced Q, while the latter steps require NAD^+. The ability of proline to maintain the F_1F_O-ATPase in the forward mode is genuinely due to the metabolism of proline through ProDH. This leads to Q reduction and the fueling of CIII. Relevant to this, duroquinone (DQ) could partially mimic the effects of proline by directly fueling CIII, but not to the same effect—as DQ is expected to exert undesirable effects such as ROS formation [44]. Several electron transfer pathways converge at the Q-junction, particularly the NADH- and succinate-linked (CI- and CII-linked) pathways, and include the glycerophosphate pathway and fatty acid oxidation pathway with electron entry through the electron-transferring flavoprotein Complex into Q as well [45]. The proline pathway through ProDH is to be added to the list of ET pathways converging at the Q-junction with potential additive effects on OXPHOS and ET capacities when operating in combination.

We found that S was the dominant α-pathway with $J_S > J_{Pro}$. With this understanding, flux control ratios are $\alpha = J_S/J_{SPro}$ and $\beta = J_{Pro}/J_{SPro}$. Additivity $A_{\check{\alpha\beta}}$ is defined as $(1 - \alpha)/\beta$ [29]. Complete additivity ($A_{\check{\alpha\beta}} = 1$) is obtained when the linear sum of the component S- and Pro-pathway flux ($J_S + J_{Pro}$) equals the flux of the convergent SPro-pathway with the SPro-substrate combination (J_{SPro}). In the OXPHOS state, $A_{\check{\alpha\beta}}$ was 2 in liver and 1.6 to 2.1 in kidney mitochondria, thereby indicating excess additivity and the synergistic activation of O_2 flux. This contrasts with the incomplete additivity of convergent NADH- and succinate-linked pathway flux [29]. LEAK respiration, however, is not linearly responsive to ET capacity, as reflected by the lower additivity observed in liver mitochondria. Surprisingly, the additivity of LEAK respiration was negative in kidney mitochondria, which implies the suppression of LEAK respiration by proline and, consequently, an overly proportional effect on coupling efficiency.

In conclusion, our data show that proline can maintain ATP production by the F_1F_O-ATPase when CI is impaired. This information should be added to an already long list

involving this amino acid in cellular bioenergetics, osmoregulation, stress protection, apoptosis, and cancer cell metabolism (reviewed in [46])—which are addressed in [5,47,48].

4. Materials and Methods

4.1. Animals

Mice were of mixed 129 Sv and C57BL/6 background. The animals used in our study were of either sex and between 2 and 6 months of age. Data obtained from liver, kidney, brain, or heart mitochondria of mice of a particular gender or age (2, 4, or 6 months) did not yield any qualitative differences, thus all data were pooled. Mice were housed in a room maintained at 20–22 °C on a 12-h light–dark cycle with food and water available ad libitum. The study was conducted according to the guidelines of the Declaration of Helsinki and were approved by the Animal Care and Use Committee of the Semmelweis University (Egyetemi Állatkísérleti Bizottság, protocol code F16-00177 [A5753-01]; date of approval: May 15, 2017).

4.2. Isolation of Mitochondria

Liver, kidney, brain, and heart mitochondria were isolated from mice as described in [36,49]. The protein concentration was determined using the bicinchoninic acid assay and calibrated using bovine serum standards [50] using a Tecan Infinite® 200 PRO series plate reader (Tecan Deutschland GmbH, Crailsheim, Germany).

4.3. Determination of Membrane Potential ($\Delta\Psi mt$) in Issolated Mitochondria

$\Delta\Psi_{mt}$ of isolated mitochondria (0.5 or 1 mg of mouse liver or kidney mitochondria in two ml buffer medium for normoxic or anoxic experiments, respectively; 0.25 or 0.5 mg of brain mitochondria per two ml of medium (the composition of which is described in [32]); 0.25 mg of mouse heart mitochondria per two ml of medium) was estimated fluorimetrically with safranine O [51] or rhodamine 123 [52] and expressed as arbitrary units or calibrated to millivolts as described in [32], acknowledging the considerations elaborated in [53,54] regarding the inhibition of respiration and unspecific binding of safranine. Fluorescence was recorded using a Hitachi F-7000 spectrofluorimeter (Hitachi High Technologies, Maidenhead, UK) at a 5-Hz acquisition rate, at 495 nm and 585 nm excitation and emission wavelengths, respectively, or the Oroboros O2k (Oroboros Instruments, Innsbruck, Austria) equipped with the O2k-Fluo LED2-Module, or the NextGen-O2k prototype equipped with the O2k-Fluo Smart Module, with optical sensors including an LED (465 nm; <505 nm short-pass excitation filter), a photodiode, and specific optical filters (>560 nm long-pass emission filter) [51]. The experiments were performed at 37 °C.

4.4. Mitochondrial Respiration

Oxygen consumption was performed polarographically using an Oxygraph-2k. A half to 1 mg of mouse liver or kidney mitochondria in two ml of buffer medium for normoxic or anoxic experiments was used, respectively; 0.25 mg of brain mitochondria per two ml of medium was used. Mitochondria were suspended in 2 ml incubation medium, the composition of which was identical to that for $\Delta\Psi_{mt}$ determination. The experiments were performed at 37 °C. The oxygen concentration (μM) and oxygen flux ($pmol \cdot s^{-1} \cdot mg^{-1}$; negative time derivative of oxygen concentration, divided by mitochondrial mass per volume and corrected for instrumental background oxygen flux arising from oxygen consumption of the oxygen sensor and back-diffusion into the chamber) were recorded using DatLab software (Versions 5.1.0.20 and 7.4.0.4, Oroboros Instruments, Innsbruck, Austria).

4.5. Determination of NADH Autofluorescence in Isolated Mitochondria

The NADH autofluorescence was measured using two different instruments: (1) Hitachi F-7000 fluorescence spectrophotometer (Hitachi High Technologies, Maidenhead, UK) and (2) the NADH-Module of the NextGen-O2k (Oroboros Instruments, Innsbruck, Austria). The NADH measurements were performed in a Hitachi F-7000 fluorescence

spectrophotometer at a 5 Hz acquisition rate, using 340 and 435 nm excitation and emission wavelengths, respectively. The NextGen-O2k allows for the simultaneous measurement of oxygen consumption and NADH autofluorescence, incorporating an ultraviolet (UV) LED with an excitation wavelength of 365 nm and an integrated spectrometer that records a wavelength range between 450 and 590 nm. The light intensity of the LED was set to 10 mA. A half a mg of mouse liver, kidney, or brain, or 0.25 mg of mouse heart mitochondria were suspended in 2 ml incubation medium, the composition of which was identical to that for $\Delta\Psi_{mt}$ determination—as described in [32]. The experiments were performed at 37 °C.

4.6. Mitochondrial Q Redox State

The coenzyme Q redox state of isolated mitochondria suspended in a buffer composition as described in [32] was followed amperometically using a three-electrode system with coenzyme Q_2 (CoQ_2, 1 μM) as a mediator, and using the Q-Module of the NextGen-O2k (Oroboros Instruments, Innsbruck, Austria). The reference electrode was Ag/AgCl/(3M KCl). The auxiliary electrode was made of platinum and the working electrode was fabricated from glassy carbon. The oxidation peak potential of CoQ_2 measured by cyclic voltammetry was set to the glassy carbon to measure the oxidation of reduced CoQ_2. The Q redox state was recorded simultaneously with O_2 flux and rhodamine 123 fluorescence.

4.7. Determination of Proline Dehydrogenase Activity

ProDH activity was determined in alamethicin-treated mitochondria immediately after isolation, as described in [53], with minor modifications. Briefly, the reaction was carried out in a 50 mM phosphate buffer (pH 7.4) with 0.25 mg mitochondria, 10 μg alamethicin, and 1 μM cytochrome c and proline concentrations, as indicated in the legends. After 30 min at 25 °C while shaking (500 rpm), the reaction was stopped by the addition of half the final volume 10 *w/v* % trichloroacetic acid and one-tenth the final volume of freshly made 0.1 M 2-aminobenzaldehyde dissolved in 40 *v/v* % ethanol. After 30 min, the absorbance on 440 nm was read against a parallel blank without substrate. The concentration of P5C was calculated using $\varepsilon = 2.58\ mM^{-1} \cdot cm^{-1}$.

4.8. Reagents

Standard laboratory chemicals, duroquinone, tetrahydro-2-furoic acid, and S-5-oxo-2-tetrahydrofurancarboxylic acid were obtained from Sigma Aldrich (St Louis, Missouri, US). SF6847 and atpenin A5 were purchased from Enzo Life Sciences (ELS AG, Lausen, Switzerland). The mitochondrial substrates were dissolved in bi-distilled water and titrated to pH 7.0 with KOH. ADP was purchased as a K^+ salt of the highest purity available (Merck KGaA, Darmstadt, Germany) and titrated to pH 6.9.

The concentrations of glutamate (G), malate (M), and oxoglutarate (Og) were always 5 mM when present. Succinate was added where indicated (S, 5 mM). ADP concentrations were 2 mM where titrations are indicated. Rotenone (Rot, 1 μM), myxothiazol (Myx, 1 μM; or 0.1 μM when specified), carboxyatractyloside (CAT, 1 μM), oligomycin (Omy, 10 μM), NaCN (CN, 1 mM), or SF6847 (SF, 1 μM; or 0.25 μM when specified) were used as indicated.

4.9. Figures on Time Courses

All traces are representative of at least three independent experiments. At the end of many experiments, the uncoupler SF6847 (SF) was added to confer a complete collapse of $\Delta\Psi_{mt}$ as a point of reference.

4.10. Statistics

Statistical analysis was performed by comparing pooled raw data using one-way ANOVA (Bonferroni test) or ANOVA on Ranks if normality failed (details in respective legends); statistical significance was accepted when $p < 0.05$ (shown as *).

Supplementary Materials: The following supporting information can be downloaded at: https://www.mdpi.com/article/10.3390/ijms23095111/s1.

Author Contributions: Methodology, T.K. and C.D.; Formal analysis, C.C.; Funding acquisition, C.C.; Investigation, G.P., S.N., D.R. and D.B.; Methodology, C.C.; Project administration, C.C.; Resources, E.G.; Supervision, C.C.; Validation, C.C.; Writing—original draft, C.C.; Writing—review & editing, E.G. and T.N.S. All authors have read and agreed to the published version of the manuscript.

Funding: This work was supported by grants from NKFIH ([TKP2021-EGA-25], FIKP-61822-64888-EATV, VEKOP 2.3.3-15-2016-00012, 2017-2.3.4-TET-RU-2017-00003, KH129567, and K135027) to C.C. and from the project NextGen-O2k (Oroboros Instruments) which has received funding from the European Union's Horizon 2020 research and innovation programme under grant agreement No. 859770.

Institutional Review Board Statement: See Section 4.1.

Data Availability Statement: Data available in a publicly accessible repository; The data presented in this study are openly available in https://zenodo.org/deposit/6323145, accessed on 28 March 2022.

Conflicts of Interest: The authors declare no conflict of interest.

Abbreviations

ALDH4A1	delta-1-pyrroline-5-carboxylate dehydrogenase
ANT	adenine nucleotide translocase
ASAT	aspartate aminotransferase
βOH	β-hydroxybutyrate
CAT	carboxyatractyloside
CI, CII, CIII, CIV	respiratory Complexes I to IV
CN	cyanide (NaCN)
DQ	duroquinone
ET	electron transfer
ETS	electron transfer system
$\Delta\Psi_{mt}$	mitochondrial membrane potential
G	glutamate
GDH	glutamate dehydrogenase
GM	glutamate & malate
GSA	glutamate semi-aldehyde
Itac	itaconate
LEAK respiration	resting respiration in the absence of ADP
M	malate
mtIM	mitochondrial inner membrane
Myx	myxothiazol
OAT	ornithine aminotransferase
Og	2-oxoglutarate (α-ketoglutarate)
OgDH	oxoglutarate dehydrogenase
Omy	oligomycin
OXPHOS capacity	respiration at kinetically saturating [ADP]
Pro	proline
ProDH	proline dehydrogenase
P5C	pyrroline-5-carboxylate
Q	mitochondrial ETS-reactive coenzyme Q
Rot	rotenone
Rox	residual oxygen consumption
S	succinate
SCS	succinate-CoA ligase (succinyl-CoA synthetase)
SF	uncoupler SF6847
S-5-oxo	S-5-oxo-2-tetrahydrofurancarboxylic acid
THFA	tetrahydro-2-furoic acid
UQ	ubiquinone, oxidized Q
UQH_2	ubiquinol, reduced Q

References

1. Taggart, J.V.; Krakaur, R.B. Studies on the cyclophorase system; the oxidation of proline and hydroxyproline. *J. Biol. Chem.* **1949**, *177*, 641–653. [CrossRef]
2. Johnson, A.B.; Strecker, H.J. The interconversion of glutamic acid and proline. IV. The oxidation of proline by rat liver mitochondria. *J. Biol. Chem.* **1962**, *237*, 1876–1882. [CrossRef]
3. McKnight, J.A.; Hird, F.J. The oxidation of proline by mitochondrial preparations. *Comp. Biochem. Physiol. Part B Comp. Biochem.* **1986**, *85*, 289–294. [CrossRef]
4. Scaraffia, P.; Wells, M. Proline can be utilized as an energy substrate during flight of Aedes aegypti females. *J. Insect Physiol.* **2003**, *49*, 591–601. [CrossRef]
5. McDonald, A.E.; Pichaud, N.; Darveau, C.-A. "Alternative" fuels contributing to mitochondrial electron transport: Importance of non-classical pathways in the diversity of animal metabolism. *Comp. Biochem. Physiol. Part B Biochem. Mol. Biol.* **2018**, *224*, 185–194. [CrossRef]
6. Gäde, G.; Auerswald, L. Beetles' choice—proline for energy output: Control by AKHs. *Comp. Biochem. Physiol. Part B Biochem. Mol. Biol.* **2002**, *132*, 117–129. [CrossRef]
7. D'Aniello, C.; Patriarca, E.J.; Phang, J.M.; Minchiotti, G. Proline Metabolism in Tumor Growth and Metastatic Progression. *Front. Oncol.* **2020**, *10*, 776. [CrossRef]
8. Phang, J.M. Proline Metabolism in Cell Regulation and Cancer Biology: Recent Advances and Hypotheses. *Antioxidants Redox Signal.* **2019**, *30*, 635–649. [CrossRef]
9. Hancock, C.N.; Liu, W.; Alvord, W.G.; Phang, J.M. Co-regulation of mitochondrial respiration by proline dehydrogenase/oxidase and succinate. *Amino Acids* **2016**, *48*, 859–872. [CrossRef]
10. Vettore, L.A.; Westbrook, R.L.; Tennant, D.A. Proline metabolism and redox; maintaining a balance in health and disease. *Amino Acids* **2021**, *53*, 1779–1788. [CrossRef]
11. Adams, E.; Frank, L. Metabolism of Proline and the Hydroxyprolines. *Annu. Rev. Biochem.* **1980**, *49*, 1005–1061. [CrossRef] [PubMed]
12. Du, J.; Zhu, S.; Lim, R.R.; Chao, J.R. Proline metabolism and transport in retinal health and disease. *Amino Acids* **2021**, *53*, 1789–1806. [CrossRef] [PubMed]
13. Meyer, J. Proline transport in rat liver mitochondria. *Arch. Biochem. Biophys.* **1977**, *178*, 387–395. [CrossRef]
14. Atlante, A.; Passarella, S.; Pierro, P.; Quagliariello, E. Proline Transport in Rat Kidney Mitochondria. *Arch. Biochem. Biophys.* **1994**, *309*, 139–148. [CrossRef] [PubMed]
15. Summitt, C.B.; Johnson, L.C.; Jönsson, T.J.; Parsonage, D.; Holmes, R.P.; Lowther, W.T. Proline dehydrogenase 2 (PRODH2) is a hydroxyproline dehydrogenase (HYPDH) and molecular target for treating primary hyperoxaluria. *Biochem. J.* **2015**, *466*, 273–281. [CrossRef] [PubMed]
16. Pandhare, J.; Donald, S.P.; Cooper, S.K.; Phang, J.M. Regulation and function of proline oxidase under nutrient stress. *J. Cell. Biochem.* **2009**, *107*, 759–768. [CrossRef] [PubMed]
17. Erecińska, M. Ubiquinone in proline oxidation. *Arch. Int. Pharmacodyn. Ther.* **1965**, *158*, 209–215.
18. Chinopoulos, C. The "B space" of mitochondrial phosphorylation. *J. Neurosci. Res.* **2011**, *89*, 1897–1904. [CrossRef]
19. Kowaloff, E.; Granger, A.; Phang, J. Alterations in proline metabolic enzymes with mammalian development. *Metabolism* **1976**, *25*, 1087–1094. [CrossRef]
20. Schmidt, J.A.; Rinaldi, S.; Scalbert, A.; Ferrari, P.; Achaintre, D.; Gunter, M.J.; Appleby, P.N.; Key, T.J.; Travis, R.C. Plasma concentrations and intakes of amino acids in male meat-eaters, fish-eaters, vegetarians and vegans: A cross-sectional analysis in the EPIC-Oxford cohort. *Eur. J. Clin. Nutr.* **2016**, *70*, 306–312. [CrossRef]
21. McMenamy, R.H.; Lund, C.C.; Oncley, J.L. Unbound Amino Acid Concentrations in Human Blood Plasmas. *J. Clin. Investig.* **1957**, *36*, 1672–1679. [CrossRef] [PubMed]
22. Frame, E.G. The Levels of Individual Free Amino Acids in the Plasma of Normal Man at Various Intervals After a High-Protein Meal1. *J. Clin. Investig.* **1958**, *37*, 1710–1723. [CrossRef] [PubMed]
23. Martinez-Banaclocha, M.; Frank, A.; Diez-Tejedor, E.; Hernanz, A. Amino acid concentrations in cerebrospinal fluid and serum in Alzheimer's disease and vascular dementia. *J. Neural Transm.* **1993**, *6*, 1–9. [CrossRef] [PubMed]
24. Liu, Z.; Jeppesen, P.B.; Gregersen, S.; Larsen, L.B.; Hermansen, K. Chronic Exposure to Proline Causes Aminoacidotoxicity and Impaired Beta-Cell Function: Studies In Vitro. *Rev. Diabet. Stud.* **2016**, *13*, 66–78. [CrossRef]
25. Newton, H.; Wang, Y.-F.; Camplese, L.; Mokochinski, J.B.; Kramer, H.B.; Brown, A.E.X.; Fets, L.; Hirabayashi, S. Systemic muscle wasting and coordinated tumour response drive tumourigenesis. *Nat. Commun.* **2020**, *11*, 4653. [CrossRef]
26. Scharff, R.; Wool, I.G. Effect of diabetes on the concentration of amino acids in plasma and heart muscle of rats. *Biochem. J.* **1966**, *99*, 173–178. [CrossRef]
27. Németh, B.; Doczi, J.; Csete, D.; Kacso, G.; Ravasz, D.; Adams, D.; Kiss, G.; Nagy, A.M.; Horvath, G.; Tretter, L.; et al. Abolition of mitochondrial substrate-level phosphorylation by itaconic acid produced by LPS-induced Irg1 expression in cells of murine macrophage lineage. *FASEB J.* **2016**, *30*, 286–300. [CrossRef]
28. Gnaiger, E. Mitochondrial Pathways and Respiratory Control. An introduction to OXPHOS analysis 5th ed. *Bioenerg. Commun.* **2020**, *2020*, 2. [CrossRef]
29. Gnaiger, E.; MitoEAGLE Task Group. Mitochondrial physiology. *Bioenerg. Commun.* **2020**, *2020*, 1–44. [CrossRef]

30. Luo, M.; Arentson, B.W.; Srivastava, D.; Becker, D.F.; Tanner, J.J. Crystal Structures and Kinetics of Monofunctional Proline Dehydrogenase Provide Insight into Substrate Recognition and Conformational Changes Associated with Flavin Reduction and Product Release. *Biochemistry* **2012**, *51*, 10099–10108. [CrossRef]
31. Scott, G.K.; Yau, C.; Becker, B.C.; Khateeb, S.; Mahoney, S.; Jensen, M.B.; Hann, B.; Cowen, B.J.; Pegan, S.D.; Benz, C.C. Targeting Mitochondrial Proline Dehydrogenase with a Suicide Inhibitor to Exploit Synthetic Lethal Interactions with p53 Upregulation and Glutaminase Inhibition. *Mol. Cancer Ther.* **2019**, *18*, 1374–1385. [CrossRef] [PubMed]
32. Chinopoulos, C.; Gerencser, A.A.; Mandi, M.; Mathe, K.; Töröcsik, B.; Doczi, J.; Turiak, L.; Kiss, G.; Konràd, C.; Vajda, S.; et al. Forward operation of adenine nucleotide translocase during F0F1-ATPase reversal: Critical role of matrix substrate-level phosphorylation. *FASEB J.* **2010**, *24*, 2405–2416. [CrossRef] [PubMed]
33. Chinopoulos, C. Mitochondrial consumption of cytosolic ATP: Not so fast. *FEBS Lett.* **2011**, *585*, 1255–1259. [CrossRef] [PubMed]
34. Klingenberg, M. The ADP and ATP transport in mitochondria and its carrier. *Biochim. Biophys. Acta (BBA)—Biomembr.* **2008**, *1778*, 1978–2021. [CrossRef] [PubMed]
35. Alexandre, A.; Reynafarje, B.; Lehninger, A.L. Stoichiometry of vectorial H^+ movements coupled to electron transport and to ATP synthesis in mitochondria. *Proc. Natl. Acad. Sci. USA* **1978**, *75*, 5296–5300. [CrossRef]
36. Kiss, G.; Konrad, C.; Doczi, J.; Starkov, A.A.; Kawamata, H.; Manfredi, G.; Zhang, S.F.; Gibson, G.E.; Beal, M.F.; Adam-Vizi, V.; et al. The negative impact of α-ketoglutarate dehydrogenase complex deficiency on matrix substrate-level phosphorylation. *FASEB J.* **2013**, *27*, 2392–2406. [CrossRef]
37. Bui, D.; Ravasz, D.; Chinopoulos, C. The Effect of 2-Ketobutyrate on Mitochondrial Substrate-Level Phosphorylation. *Neurochem. Res.* **2019**, *44*, 2301–2306. [CrossRef] [PubMed]
38. Chinopoulos, C.; Tretter, L.; Adam-Vizi, V. Depolarization of in Situ Mitochondria Due to Hydrogen Peroxide-Induced Oxidative Stress in Nerve Terminals: Inhibition of alpha-ketoglutarate dehydrogenase. *J. Neurochem.* **2002**, *73*, 220–228. [CrossRef] [PubMed]
39. Martinez-Reyes, I.; Diebold, L.P.; Kong, H.; Schieber, M.; Huang, H.; Hensley, C.T.; Mehta, M.; Wang, T.; Santos, J.H.; Woychik, R.; et al. TCA Cycle and Mitochondrial Membrane Potential Are Necessary for Diverse Biological Functions. *Mol. Cell* **2016**, *61*, 199–209. [CrossRef]
40. Vafai, S.B.; Mevers, E.; Higgins, K.W.; Fomina, Y.; Zhang, J.; Mandinova, A.; Newman, D.; Shaw, S.Y.; Clardy, J.; Mootha, V.K. Natural Product Screening Reveals Naphthoquinone Complex I Bypass Factors. *PLoS ONE* **2016**, *11*, e0162686. [CrossRef]
41. Ravasz, D.; Kacso, G.; Fodor, V.; Horvath, K.; Adam-Vizi, V.; Chinopoulos, C. Reduction of 2-methoxy-1,4-naphtoquinone by mitochondrially-localized Nqo1 yielding NAD+ supports substrate-level phosphorylation during respiratory inhibition. *Biochim. Biophys. Acta* **2018**, *1859*, 909–924. [CrossRef] [PubMed]
42. Zieliński, Ł.P.; Smith, A.C.; Smith, A.G.; Robinson, A.J. Metabolic flexibility of mitochondrial respiratory chain disorders predicted by computer modelling. *Mitochondrion* **2016**, *31*, 45–55. [CrossRef] [PubMed]
43. Fato, R.; Bergamini, C.; Leoni, S.; Lenaz, G. Mitochondrial production of reactive oxygen species: Role of Complex I and quinone analogues. *BioFactors* **2008**, *32*, 31–39. [CrossRef] [PubMed]
44. Tanner, J.J.; Fendt, S.-M.; Becker, D.F. The Proline Cycle As a Potential Cancer Therapy Target. *Biochemistry* **2018**, *57*, 3433–3444. [CrossRef]
45. Chinopoulos, C.; Vajda, S.; Csanády, L.; Mándi, M.; Mathe, K.; Adam-Vizi, V. A Novel Kinetic Assay of Mitochondrial ATP-ADP Exchange Rate Mediated by the ANT. *Biophys. J.* **2009**, *96*, 2490–2504. [CrossRef]
46. Smith, P.K.; Krohn, R.I.; Hermanson, G.T.; Mallia, A.K.; Gartner, F.H.; Provenzano, M.D.; Fujimoto, E.K.; Goeke, N.M.; Olson, B.J.; Klenk, D.C. Measurement of protein using bicinchoninic acid. *Anal. Biochem.* **1985**, *150*, 76–85. [CrossRef]
47. Åkerman, K.E.; Wikström, M.K. Safranine as a probe of the mitochondrial membrane potential. *FEBS Lett.* **1976**, *68*, 191–197. [CrossRef]
48. Emaus, R.K.; Grunwald, R.; Lemasters, J.J. Rhodamine 123 as a probe of transmembrane potential in isolated rat-liver mitochondria: Spectral and metabolic properties. *Biochim. Biophys. Acta* **1986**, *850*, 436–448. [CrossRef]
49. Valle, V.G.; Pereira-Da-Silva, L.; Vercesi, A.E. Undesirable feature of safranine as a probe for mitochondrial membrane potential. *Biochem. Biophys. Res. Commun.* **1986**, *135*, 189–195. [CrossRef]
50. Chinopoulos, C.; Adam-Vizi, V. Mitochondrial Ca^{2+} sequestration and precipitation revisited. *FEBS J.* **2010**, *277*, 3637–3651. [CrossRef]
51. Krumschnabel, G.; Eigentler, A.; Fasching, M.; Gnaiger, E. Use of Safranin for the Assessment of Mitochondrial Membrane Potential by High-Resolution Respirometry and Fluorometry. *Methods Enzymol.* **2014**, *542*, 163–181. [CrossRef] [PubMed]
52. Komlódi, T.C.L.; Doerrier, C.; Moore, A.L.; Rich, P.R.; Gnaiger, E. Coupling and pathway control of coenzyme Q redox state and respiration in isolated mitochondria. *Bioenerg. Commun.* **2021**, *2021*. [CrossRef]
53. Kawabata, Y.; Katunuma, N.; Sanada, Y. Characteristics of Proline Oxidase in Rat Tissues. *J. Biochem.* **1980**, *88*, 281–283. [CrossRef] [PubMed]
54. Mezl, V.A.; Knox, W.E. Properties and analysis of a stable derivative of pyrroline-5-carboxylic acid for use in metabolic studies. *Anal. Biochem.* **1976**, *74*, 430–440. [CrossRef]